1 Seasonal temperature variation influences climate suitability for dengue, 2 chikungunya, and Zika transmission 3 John H. Huber^{1, 2}, Marissa L. Childs³, Jamie M. Caldwell², Erin A. Mordecai^{2*} 4 5 ¹Department of Applied and Computational Mathematics and Statistics, University 6 of Notre Dame, Notre Dame, Indiana, USA 7 ²Department of Biology, Stanford University, Stanford, California, USA 8 ³Emmett Interdisciplinary Program in Environment and Resources, Stanford 9 University, Stanford, California, USA 10 11 *Corresponding Author: emordeca@stanford.edu 12 13 Short title: Seasonal climate affects vector transmission

ABSTRACT

14

15

16

17

18

19

20

21

22

23

24

25

26

27

28

29

30

31

32

33

34

35

36

Dengue, chikungunya, and Zika virus epidemics transmitted by Aedes aegypti mosquitoes have recently (re)emerged and spread throughout the Americas, Southeast Asia and the Pacific Islands, and elsewhere. Understanding how environmental conditions affect epidemic magnitude and duration is critical for predicting and responding to the geographic and seasonal spread of disease. Here, we develop the first dynamic disease transmission model for dengue virus and Aedes aegypti mosquitoes that integrates mechanistic, empirically parameterized. and independently validated mosquito and virus trait thermal responses under seasonally varying temperatures. With the model, we examine the influence of variation in seasonal temperature regime on epidemic dynamics. We find that at both constant and seasonally varying temperatures, warmer temperatures at the start of epidemics promote more rapid epidemics due to faster burnout of the susceptible population. By contrast, intermediate temperatures ($\sim 24^{\circ}$ C) at epidemic onset produced the largest epidemics in a seasonally varying temperature regime. When seasonal temperature variation was low, 25-35°C annual average temperatures produced the largest epidemics, but this range shifts to cooler temperatures as seasonal temperature variation increases. Tropical and subtropical cities such as Rio de Janeiro, Fortaleza, and Salvador, Brazil; Cali, Cartagena, and Baranquilla, Colombia; Delhi, India; Guangzhou, China; and Manila, Philippines have mean annual temperatures and seasonal temperature ranges that produce the largest epidemics. However, more temperate cities like Shanghai, China had high epidemic suitability because large seasonal variation offset moderate annual

38

39

40

41

42

43

44

45

46

47

48

49

50

51

52

53

54

55

56

57

58

average temperatures. By accounting for seasonal variation in temperature, our model provides a baseline for mechanistically understanding environmental suitability for virus transmission by *Aedes aegypti*. Overlaying the impact of human activities and socioeconomic factors onto this mechanistic temperature-dependent framework is critical for understanding likelihood and magnitude of outbreaks. **NON-TECHNICAL SUMMARY (150-200 WORDS)** Mosquito-borne viruses like dengue, Zika, and chikungunya have recently caused large epidemics that are partly driven by temperature. Using a mathematical model built from laboratory experimental data for *Aedes aegypti* mosquitoes and dengue virus, we examine the impact of variation in seasonal temperature regimes on epidemic size and duration. At constant temperatures, both low and high temperatures (20°C and 35°C) produce small epidemics, while intermediate temperatures like 25°C and 30°C produce much larger epidemics. In seasonally varying temperature environments, epidemics peak more rapidly at higher starting temperatures. Intermediate starting temperatures produce the largest epidemics. Seasonal mean temperatures of 25-35°C are most suitable for large epidemics when seasonality is low, but in more variable seasonal environments epidemic suitability peaks at lower annual average temperatures. Tropical and sub-tropical cities have the highest temperature suitability for epidemics, but more temperate cities with high seasonal variation also have the potential for very large epidemics.

60

61

62

63

64

65

66

67

68

69

70

71

72

73

74

75

76

77

78

79

80

81

INTRODUCTION Over the last 30-40 years, arboviral outbreaks have dominated the public health landscape globally (1). These viruses, most notably chikungunya (CHIKV), dengue (DENV), and Zika (ZIKV), can cause symptoms ranging from rash, arthralgia, and fever to hemorrhagic fever (DENV), long-term arthritis (CHIKV), Guillain-Barré syndrome and microcephaly (ZIKV) (2-4). DENV, which historically spread worldwide along shipping routes (5), places 3.97 billion individuals at risk worldwide (6) and causes an estimated 390 million cases annually, including 96 million symptomatic cases (7). CHIKV was introduced into the Americas in December 2013 after an outbreak in St. Martin Island (8). Since then, autochthonous transmission has been reported in 45 countries (9), and 1.3 billion people worldwide are at risk of contracting CHIKV (10). More recently, the ZIKV epidemic in the Americas captured global attention after the World Health Organization (WHO) designated it a Public Health Emergency of International Concern in February 2016 in response to its association with neurological disorders. Following the first reported case in Brazil in May 2015, ZIKV has spread to 48 countries and territories where it is transmitted autochthonously (11). Because DENV, CHIKV, and ZIKV are mostly transmitted by *Aedes aegypti* mosquitoes, they may have similar geographic distributions and risk factors. Informed public health decisions to limit the spread and magnitude of these arboviral epidemics depend on a robust understanding of transmission dynamics. One mechanistic modeling framework, the Susceptible – Infected – Recovered (SIR) model, has been implemented successfully to model the dynamics of outbreaks of

83

84

85

86

87

88

89

90

91

92

93

94

95

96

97

98

99

100

101

102

103

104

influenza, measles, and vector-borne diseases such as CHIKV and ZIKV (12-14). This approach tracks virus population dynamics by compartmentalizing individuals by their state in an epidemic (i.e., Susceptible (S), Infected (I), Recovered (R)). This framework can be extended to include additional compartments, such as a latency stage, or to incorporate the dynamics of the mosquito population for vector transmission. Arbovirus dynamics are strikingly seasonal and geographically restricted to relatively warm climates (15). This arises because several life history traits of the mosquitoes that transmit DENV, CHIKV, and ZIKV are strongly influenced by temperature and seasonality (16-23). For simplicity, many existing models assume static life history traits (14), and those that address seasonal forcing tend to incorporate sinusoidal variation as a single transmission parameter, β (24). However, decades of experimental work have demonstrated strongly nonlinear (often unimodal) relationships between mosquito and pathogen traits and temperature that are not well captured in a single sinusoidal forcing function (25). Efforts by Yang et al. (26,27) addressed the need to include seasonal variation by adopting an SEI-SEIR compartmental framework with time-varying entomological parameters and fitting the model to DENV incidence data in Campinas, Brazil. Here, we expand upon an SEI-SEIR model (26,27) to incorporate nonlinear, temperature-dependent vector parameters (25). We use the model to evaluate the effect of temperature on epidemic length and size, producing outputs that are more directly comparable to observed epidemics than static measures like R_0 (28). Importantly, we move beyond mean temperature to examine the impact of seasonal

temperature variation on epidemics, by allowing entomological parameters to vary seasonally with temperature. Specifically, we use the model to ask: (1) How does final epidemic size vary across constant temperatures? (2) Under seasonally varying temperatures, how does the temperature at the start of the epidemic affect the final epidemic size and duration? (3) How do temperature mean and seasonal range interact to determine epidemic size? (4) Based on the model, which geographic locations have high epidemic suitability based on climate?

METHODS

114 Model

105

106

107

108

109

110

111

112

113

120

- 115 Model Framework
- We adopted an SEI-SEIR compartmental modeling framework to simulate arboviral
- transmission by the *Aedes aegypti* vector (Fig. 1). We introduced temperature-
- dependence into the model by using fitted thermal response curves for the
- mosquito life history traits provided by Mordecai et al. (25). The full model is:

$$\frac{dS_V}{dt} = EFD(T) * pEA(T) * MDR(T) * N_V * \left(1 - \frac{N_V}{K(T)}\right) - \left(a(T) * pMI(T) * \frac{I_H}{N_U} + \mu(T)\right) * S_V$$
(1)

$$\frac{dE_V}{dt} = a(T) * pMI(T) * \frac{I_H}{N_H} * S_V - \left(PDR(T) + \mu(T)\right) * E_V$$
 (2)

$$\frac{dI_V}{dt} = PDR(T) * E_V - \mu(T) * I_V$$
(3)

$$\frac{dS_H}{dt} = -a(T) * b(T) * \frac{I_V}{N_H} * S_H$$
(4)

$$\frac{dE_H}{dt} = a(T) * b(T) * \frac{I_V}{N_H} * S_H - \delta * E_H$$
(5)

$$\frac{dI_H}{dt} = \delta * E_H - \eta * I_H \tag{6}$$

122

123

124

125

126

127

128

129

130

131

132

133

134

135

136

137

138

139

140

141

142

$$\frac{dR_H}{dt} = \eta * I_H \tag{7}$$

Fig 1 Caption. Compartmental model of transmission. S_H , E_H , I_H , and R_H represent the susceptible, exposed (or latent), infectious, and recovered segments of the human population, respectively. Likewise, S_V , E_V , and I_V represent the susceptible, exposed (or latent), and infectious segments of the mosquito population. Solid arrows signify the directionality of transition from one compartment to the next, and dashed arrows indicate the directionality of transmission. The SEI portion of the model describes the vector population, where S_V represents the number of susceptible mosquitoes, E_V is the number of mosquitoes in the latency stage, and I_V is the number of infectious mosquitoes. We assumed that Aedes aeavpti mosquitoes remain infectious until they die. In equations 1-3. EFD(T) is the number of eggs laid per female per day, pEA(T) is the probability of mosquito egg-to-adult survival, MDR(T) is the mosquito egg-to-adult development rate, N_V is the total mosquito population at time t (i.e., $S_v + E_v + I_v$), K(T) is the carrying capacity for the mosquito population, a(T) is the per mosquito biting rate, pMI(T) is the probability of mosquito infection per bite on an infectious host, $\mu(T)$ is the adult mosquito mortality rate, and PDR(T) is the parasite development rate. Each life history trait of the *Aedes aegypti* mosquito is a temperature-dependent function fit from experimental laboratory data (Table 1).

Table 1. Fitted thermal responses for *Aedes aegypti* life history traits. Traits were fit to a Brière $[cT(T-T_0)(T_m-T)^{\frac{1}{2}}]$ or a quadratic $[c(T-T_m)(T-T_0)]$ function where T represents temperature. T_0 and T_m are the critical thermal minimum and maximum, respectively, and c is the rate constant. Thermal responses were fit by (29).

Trait	Definition	Function	Fitted Parameters		
а	Biting rate (day ⁻¹)	Brière	c = 2.71e-04	$T_{min}=14.67$	$T_{max} = 41.00$
EFD	Eggs laid per female per day	Brière	<i>c</i> = 2.08e-02	$T_{min}=14.06$	$T_{max} = 32.03$
рEA	Probability of mosquito egg-to- adult survival	Quadratic	<i>c</i> = -3.36e-03	$T_{min} = 7.68$	$T_{max} = 38.31$
MDR	Mosquito egg-to-adult development rate (day ⁻¹)	Brière	<i>c</i> = 1.49e-04	$T_{min} = 15.12$	$T_{max} = 37.67$
lf	Adult mosquito lifespan (days)	Quadratic	c = -1.24e+00	$T_{min} = 16.63$	$T_{max} = 31.85$
b	Probability of mosquito infectiousness	Brière	<i>c</i> = 9.86e-04	$T_{min} = 12.05$	$T_{max} = 32.79$
рМI	Probability of mosquito infection	Brière	<i>c</i> = 5.23e-04	$T_{min}=1.51$	$T_{max} = 34.74$
PDR	Virus extrinsic incubation rate (day-1)	Brière	c = 1.04e-04	$T_{min} = 11.50$	$T_{max} = 38.97$

The SEIR portion of the model describes the human population, where S_H represents the number of susceptible individuals, E_H the number of latent (or exposed) individuals, I_H the number of infectious individuals, and R_H the number of recovered individuals. We assumed a static population size, N_H , that was neither subject to births nor deaths because the human lifespan far exceeds the duration of

an epidemic. Further, we binned asymptomatic and symptomatic individuals into a single infectious class since asymptomatic infections have been shown to transmit DENV (30) and exhibit similar viremic profiles as symptomatic patients in CHIKV (31). Based on previous arboviral outbreaks (32,33), we assumed that an infection conferred long-term immunity to an individual. Thus, a previously infectious individual entering the recovered class is protected from subsequent re-infection for the remainder of the epidemic. In the case of dengue, where there are four unique serotypes, we consider single-season epidemics of a single serotype. In equations 4-7, b(T) is the probability of human infection per bite by an infectious mosquito, δ^{-1} is the intrinsic incubation period, and η^{-1} is the human infectivity period. Since human components of the transmission cycle are not seasonal, we used constants of 5.9 days for the intrinsic incubation period, $1/\delta$, and 5.0 days for the infectious period, $1/\eta$ (34). All temperature-independent parameter values are given in Table 2.

Table 2. Values of temperature-invariant parameters used in the model, and their sources.

Parameter	Definition	Value	Source
δ^{-1}	Intrinsic incubation period (days)	5.9	(34)
η^{-1}	Human infectivity period (days)	5.0	(34)
$I_0^H/_N$	Proportion of initially infectious humans	0.0025	(34)
$I_0^V/_M$	Proportion of initially infectious mosquitoes	0.015	(34)

M/N Ratio of mosquitoes-to-humans at 29°C 2.0 (35)

Further, because the lifespan of an adult mosquito is short relative to the timespan of an epidemic, we allowed mosquito birth and death rates to drive population dynamics. Additionally, the birth rate of susceptible mosquitoes was regulated by a temperature-dependent carrying capacity, K (equation 8), which we modeled as a modified Arrhenius equation (36):

$$K(T) = \frac{EFD(T_0) * pEA(T_0) * MDR(T_0) - \mu(T_0)}{EFD(T_0) * pEA(T_0) * MDR(T_0)} * N_m * e^{\frac{-E_A * (T - T_0)^2}{K_B * (T + 273) * (T_0 + 273)}}$$
(8)

Here, T_0 is defined as the reference temperature (i.e., the temperature at which the carrying capacity is greatest) in Celsius, N_m is the maximum carrying capacity, and κ_B is Boltzmann constant (8.617 x 10^{-5} eV/K). *EFD* is the number of eggs laid per female per day, pEA is the probability of egg-to-adult mosquito survival, MDR is the mosquito egg-to-adult development rate, and μ is the adult mosquito mortality rate. We calculated these values for the reference temperature. E_A is the activation energy, which we set to 0.5 and represents the temperature dependence of the carrying capacity, a conservative estimate as we lacked sufficient data on estimates of the carrying capacity of *Aedes aegypti* and its underlying temperature dependence. To convert from Celsius to Kelvin, we incremented the temperature T and the reference temperature T_0 by 273. Equation (8) was adopted from (36) and modified to allow the distribution to be unimodal. We set the reference temperature, T_0 , to 29°C, the optimal transmission temperature for *Aedes aegypti* transmission found by Mordecai et al. (25).

Seasonal Forcing

193

194

To address seasonality in the model, we allowed temperature to vary over time. We modeled temperature as a sinusoidal curve with a period of 365 days of the form:

$$T(t) = \frac{T_{max} - T_{min}}{2} * \sin\left(\frac{2\pi}{365}t\right) + T_{mean}$$
(9)

Here, T_{max} , T_{mean} , and T_{min} represent the average monthly maximum, mean, and minimum temperatures across a calendar year, respectively, and t is measured in days. By modeling temperature as a function of time, we allowed the life history traits of the *Aedes aegypti* vector to vary across time for the duration of the epidemic.

204 **Data**

203

212

- 205 Life History Traits
- To incorporate seasonal forcing into the compartmental modeling framework, we
- used fitted mechanistic thermal response curves (25). Mordecai et al. (25) examined
- 208 published data on thermal responses for life history traits of the *Aedes aegypti*
- vector and adopted a Bayesian approach for fitting quadratic (Q(T); Eq. 10) or
- 210 Brière (B(T); Eq. 11) curves.

$$Q(T) = c * (T - T_{min}) * (T - T_{max})$$
(10)

$$B(T) = c * T * (T - T_{min}) * \sqrt{T_{max} - T}$$
(11)

Here, c is a rate constant, T_{min} is the critical temperature minimum, and T_{max} is the

critical temperature maximum. Fitted parameters for each of the traits used in the

214

215

216

217

218

219

220

221

222

223

224

225

226

227

228

229

230

231

232

233

234

235

model are provided in Table 1. Consistent with Mordecai et al. (25) we assumed values above and below the critical thermal maxima and minima, respectively, were equal to zero. By doing so, we constrained the distribution of each life history trait to biologically relevant and empirically driven measures. Mordecai et al. (25) provided a fitted thermal response for adult mosquito lifespan (Table 1), which is equal to the inverse of the adult mosquito mortality rate (μ) , in days⁻¹, used in our model. At temperatures greater than or equal to the critical thermal maximum and less than or equal to the critical thermal minimum, adult mosquito mortality was set to 24 days⁻¹ (i.e., mosquitoes survive for one hour at temperatures outside of the T_{min} to T_{max} range). Historical Weather Data To identify areas of epidemic suitability across the globe, we extracted monthly mean temperatures for 2016 from Weather Underground (wunderground.com) for twenty different cities (Table 3). For each city, we calculated the mean, minimum, and maximum from the average monthly mean temperatures, to estimate temperature seasonality. This provided a range of the average monthly temperature over the span of a calendar year. We chose this time period because it provided the most recent full calendar year to demonstrate seasonal fluctuations in temperature. **Table 3.** Estimates of epidemic suitability for major cities. Epidemic suitability was calculated as the proportion of the population that became infected in simulations

run under default conditions (see Appendix). Each city was simulated with its respective temperature regime from the 2016 calendar year.

237

City	Annual Mean	Annual	Epidemic Suitability
	Temperature (°C)	Temperature	
		Amplitude (°C)	
Buenos Aires, Argentina	16.5	8.0	0.0313
Sao Paulo, Brazil	20.6	5.0	0.509
Rio de Janeiro, Brazil	24.3	4.0	0.999
Salvador, Brazil	26.3	2.0	0.998
Fortaleza, Brazil	27.8	0.50	0.999
Belo Horizonte, Brazil	21.9	3.0	0.499
Recife, Brazil	27.2	1.5	0.999
Shanghai, China	17.6	12.5	0.993
Beijing, China	12.8	16	0.405
Guangzhou, China	22.9	8.0	0.999
Bogotá, Colombia	14.7	1.0	0.0025
Medellin, Colombia	17.9	1.0	0.00484
Cali, Colombia	25.1	1.5	0.986
Barranquilla, Colombia	28.8	1.0	1.00
Cartagena, Colombia	28.6	1.0	1.00
Delhi, India	26.3	9.5	0.926
Tokyo, Japan	17.0	10.5	0.621

Kobe, Japan	17.4	11	0.899
Manila, Philippines	29.0	1.5	1.00
New York, USA	13.8	12	0.0328

Variability in Epidemic Dynamics with Constant Temperature

We first examined how epidemic dynamics varied across different constant temperatures. Here, we did not introduce seasonal forcing into the model but rather assumed static life history traits for *Aedes aegypti* for the simulation period. We simulated the model under default starting conditions (see Appendix) at different constant temperatures ranging from 0.0°C to 40.0°C in increments of 0.1°C.

Variability in Epidemic Dynamics with Starting Temperature

Using the model that included seasonal variation in temperature, we examined how the dynamics of an epidemic varied due to the temperature at which the epidemic began under two temperature regimes. To address this variation, we set T_{max} = 40.0° C, T_{mean} = 25.0° C, and T_{min} = 10.0° C in the time-varying seasonal temperature model under default parameters provided in the Appendix. We then varied the temperature at the start of the epidemic from 10.0° C to 40.0° C in increments of 0.1° C and examined the response of final epidemic size, epidemic length, and maximum number of infected individuals at any given point in time. We then considered the temperature regime with T_{max} = 30.0° C, T_{mean} = 25.0° C, and T_{min} = 20.0° C. The same metrics were computed using the time-varying seasonal

259

260

261

262

263

264

265

266

267

268

269

270

271

272

273

274

275

276

277

278

279

temperature module with the same parameterization while varying the start of the epidemic from 20.0°C to 30.0°C in increments of 0.1°C Seasonal Variability of Final Epidemic Size Using the compartmental modeling framework with the default starting conditions, we examined the variation in final epidemic size as a result of seasonal forcing. To do so, we simulated over a wide range of temperature mean and seasonal variance regimes. The mean annual temperature varied from 0.0°C to 40.0°C in increments of 0.1° C, while the seasonal fluctuation about the mean (i.e., $\frac{T_{max}-T_{min}}{2}$) ranged from 0.0°C to 20.0°C in increments of 0.1°C. Many of these temperature regimes are unlikely to be observed empirically. However, the simulated temperature regimes spanned the full range of feasible temperature conditions. We recorded the final epidemic size, measured as the number of individuals in the recovered compartment at the end of the simulation, for each unique combination of mean annual temperature and seasonal fluctuation. We then compared simulated climate regimes with actual climates in major cities, to measure relative epidemic suitability of the following cities: São Paulo, Brazil; Rio de Janeiro, Brazil; Salvador, Brazil; Fortaleza, Brazil; Belo Horizonte, Brazil; Recife, Brazil; Bogotá, Colombia; Medellín, Colombia; Cali, Colombia; Barranquilla, Colombia; Cartagena, Colombia; Tokyo, Japan; Delhi, India; Manila, Philippines; Shanghai, China; Beijing, China; New York City, USA; Guangzhou, China; Kobe, Japan; and Buenos Aires, Argentina. These cities were chosen because they

281

282

283

284

285

286

287

288

289

290

291

292

293

294

295

296

297

298

299

300

301

represent some of the most populous urban areas across South America and throughout the world. **Model Sensitivity and Uncertainty Analysis** To characterize uncertainty in the model, we simulated epidemic suitability at a constant temperature, ranging from 0.0°C to 40.0°C in increments of 0.5°C, while sampling 1,000 estimates for c, T_{min} , and T_{max} for each life history trait from the marginal posterior distributions provided by Mordecai et al. (25). We calculated the 95% credible interval for the epidemic suitability at each temperature. **RESULTS** Variability in Epidemic Dynamics with Constant Temperature Holding temperature constant, we examined variability in epidemic dynamics across four temperatures: 20°C, 25°C, 30°C, and 35°C. As temperature increased from 20°C to 30°C, the number of susceptible individuals depleted more rapidly (Fig. 2, S_H). At 20°C and 35°C, the epidemics were small and burned out rapidly. Although simulations run at 25°C and 30°C produced similar final epidemic sizes of 92.96% vs. 99.95% of the population infected, respectively (Fig. 2, R_H), the epidemic peaked much faster at 30°C. Finally, smaller epidemics of 1.51% and 6.17% of the population infected occurred at 20°C and 35°C.

303

304

305

306

307

308

309

310

311

312

313

314

315

316

317

318

319

320

321

322

323

Fig 2 Caption. Variation in epidemic dynamics by temperature. The model was simulated under default parameters at four constant temperatures: 20°C, 25°C, 30°C, and 35°C. The number of humans in each compartment is represented on a log scale. Variability in Epidemic Dynamics with Starting Temperature Next, we examined variability in epidemic dynamics due to the temperature at which the epidemic began, given two fixed temperature regimes (25°C mean and amplitude of either 5°C or 15°C). Consequently, starting temperature was allowed to vary from 10°C to 40°C or 20°C to 30°C depending on the regime. Given that an epidemic occurred, epidemic length monotonically decreased as a function of starting temperature for both temperature regimes (Fig. 3): warmer temperatures at the start of the epidemic produced shorter epidemics, and vice versa. When temperature varied from 10°C to 40°C, the longest epidemic simulated was 134.97 days and occurred at starting temperatures of 11.3°C and 11.4°C, and the shortest epidemic lasted 16.09 days and occurred when the temperature at the epidemic start was less than 10.3°C. When the temperature was 35.9°C or higher, no epidemic was observed. Similarly, when temperature was constrained between 20°C and 30°C, the longest epidemic simulated was 112.9 days at a starting temperature of 20°C, and the shortest epidemic lasted 71.3 days at a starting temperature of 30°C.

325

326

327

328

329

330

331

332

333

334

335

336

337

338

339

340

341

342

343

344

345

346

Fig 3 Caption. Epidemiological indices as a function of starting temperature, within a given seasonal temperature regime. The red curve represents the maximum number of humans in the infected class (I_H) at any given point during the simulation. The blue curve represents the final (or cumulative) epidemic size (R_H at the final time step). The green curve represents the length of the epidemic (i.e., the point at which the number of infected individuals was below one). Here, simulations were run with the temperature conditions: $T_{min} = 10^{\circ}$ C, $T_{mean} = 25^{\circ}$ C, and $T_{max} = 40^{\circ}$ C (A) and $T_{min} = 20$ °C, $T_{mean} = 25$ °C, and $T_{max} = 30$ °C (B). In contrast to epidemic length, both final epidemic size and maximum infected responded unimodally to the temperature at the epidemic onset. The total number of people infected peaked at a starting temperature of 24.1°C for both temperature regimes (Fig. 3). The maximum instantaneous number of infected individuals peaked at 24.4°C in both temperature regimes, with 8.42% of the population infected. Together, these results show that epidemics introduced at different times within identical seasonal temperature regimes produce dramatically different final sizes and maximum infection rates. Seasonal Variability of Final Epidemic Size To address how mean temperature and seasonal variance combined to influence the final epidemic size, we simulated over a wide range of temperature regimes that accounted for variation in the mean and temperature range over a calendar year.

348

349

350

351

352

353

354

355

356

357

358

359

360

361

362

363

364

365

366

367

368

369

We calculated relative epidemic suitability, defined as the final epidemic size as a proportion of the human population, for twenty major cities worldwide (Table 3). In a constant thermal environment, a band of mean temperatures between approximately 25°C and 35°C supports the highest epidemic suitability (Fig. 4). As the seasonal temperature range increases, lower mean temperatures are capable of supporting large epidemics. However, outside this narrow band of temperature regimes, epidemic suitability rapidly diminishes and most temperature regimes did not produce epidemics. Fig 4 Caption. Variation in epidemic suitability across different seasonal **temperature regimes.** The heat map shows the epidemic suitability (represented as the proportion of the total human population infected during an epidemic) as a function of mean annual temperature and temperature range. Here, temperature range is defined as the seasonal fluctuation about the annual mean temperature. Twenty large, globally important cities are plotted to illustrate their epidemic suitability. Of the focal 20 major cities, those with high mean temperature and small average temperature fluctuations exhibited the highest epidemic suitability. For instance, Manila, Philippines, which has a monthly mean temperature of 29°C and average seasonal amplitude in mean temperature of 1.50°C, had an epidemic suitability of 1.00. Cartagena and Barranquilla, Colombia also had epidemic suitability of 1.00. On the other hand, areas with low average temperature and

371

372

373

374

375

376

377

378

379

380

381

382

383

384

385

386

387

388

389

390

391

392

greater temperature fluctuations, such as Beijing and New York, exhibited lower but still non-zero—epidemic suitabilities of 0.405 and 0.0328 respectively. Notably, Guangzhou and Shanghai, China have high epidemic suitability (0.999 and 0.993, respectively) despite high seasonal variation in temperature due to more moderate mean temperatures (22.9 and 17.6°C, respectively), while high seasonal variation reduced suitability to 0.926 in Delhi, India, which has a high mean temperature of 26.3°C (Fig. 4). **Model Sensitivity and Uncertainty Analysis** Within the 95% credible interval previously estimated for each trait thermal response (25), epidemic suitability as a function of temperature is not highly sensitive to the values of c, T_{min} , and T_{min} (Fig. 5). The 95% credible interval on epidemic suitability across a range of constant temperatures is narrow, suggesting low uncertainty in the predicted final epidemic sizes arising from trait thermal responses. Fig 5 Caption. Sensitivity of epidemic suitability to the parameterization of life **history traits.** Epidemic suitability (represented as the proportion of the total human population infected during an epidemic) as a function of a constant temperature. Temperature was held constant, and 1,000 samples of c, T_{min} , and T_{max} were taken from the marginal posterior distribution of each trait thermal response from Mordecai et al. (25). The 95% credible interval is represented by the shaded blue region, and the median is plotted in blue.

394

395

396

397

398

399

400

401

402

403

404

405

406

407

408

409

410

411

412

413

414

DISCUSSION Recent outbreaks of DENV, CHIKV, and ZIKV in Latin America and across the globe have captured the attention of the public health community and underscore the importance of preparation for future outbreaks. As temperatures rise, the global landscape suitable for such outbreaks will expand and shift geographically, potentially placing a larger proportion of the world's population at risk. Understanding how local temperature regimes govern epidemic dynamics becomes increasingly important in resource allocation and control interventions (37). Epidemic duration and size (i.e., proportion of individuals who eventually become infected) are two key metrics of epidemic dynamics. We explored how epidemic size and duration varied across temperature regimes by extending a mechanistic modeling framework developed by (26) to incorporate nonlinear thermal responses of vector traits and seasonal forcing (25). We found that the temperature mean, seasonal variation, and seasonal timing of epidemic onset differentially affected epidemic size versus duration. The most notable variation in epidemic dynamics at constant temperature was in the rate at which susceptible individuals were depleted. Epidemics simulated at 25°C and 30°C produced similar final epidemic sizes despite the epidemic at 25°C proceeding at a much slower rate. This "slow burn" phenomenon occurs because slower depletion of susceptible individuals can produce epidemics of similar size to epidemics that infect people very rapidly.

416

417

418

419

420

421

422

423

424

425

426

427

428

429

430

431

432

433

434

435

436

437

Within a given seasonal temperature regime, epidemic size peaked at intermediate starting temperatures (24.1°C for the regimes simulated here). More generally, the unimodal relationship suggests that even in highly suitable seasonal environments, epidemics may vary dramatically depending on when they begin. Compared to epidemic size, the maximum number of infected individuals at a time peaked at slightly higher intermediate starting temperatures. We attribute this difference between the optimal temperatures for final epidemic size and the maximum number of infected individuals to the "slow burn" phenomenon: larger epidemics occurred at slightly lower starting temperatures than the instantaneous maximum number of people infected because the former epidemics last longer. Epidemic suitability was sensitive to the interaction between annual mean temperatures and seasonal temperature variation. At low seasonal amplitude, we found a narrow band of annual mean temperatures (approximately 25-35°C) with the highest epidemic suitability. Outside this band of temperature regimes, suitability diminishes rapidly. Larger seasonal variation in temperature lowers the range of optimal annual mean temperatures (i.e., suitability is high in cooler places with larger seasonal variation in temperature). It is important to note that these epidemic suitabilities should be treated as an upper bound on the potential for large epidemics. That is, within highly suitable climate regimes, epidemics can vary in magnitude due to human population size and movement dynamics (38), effective vector control, and other mitigating factors. Likewise, our estimates are conditioned on an *Aedes aegypti* population being present and virus introduction to support an outbreak.

439

440

441

442

443

444

445

446

447

448

449

450

451

452

453

Previous modeling efforts have addressed seasonal forcing by allowing transmission parameters to vary sinusoidally (24). This assumption of sinusoidal variation does not fully capture the nonlinear relationship between vector traits and temperature. Our mechanistic modeling framework provides the most comprehensive treatment of nonlinear, seasonally varying temperature-dependence for *Ae. aegypti* virus transmission to date. To do so, it incorporates experimentally measured thermal responses for all transmission-relevant vector traits into a dynamic transmission model, and these traits are forced with realistic seasonal temperature variation. To aid future studies in adopting this framework, code is available online to reproduce our results and to expand on this seasonal arboviral transmission model. Accurately describing epidemic dynamics of emerging and established vector-borne pathogens will ultimately require integrating realistic models of environmental suitability, as presented here, with demographic, social, and economic factors that promote or limit disease transmission (39).

REFERENCES

454

- 455 1. Gubler DJ. The Global Emergence / Resurgence of Arboviral Diseases As Public Health 456 Problems. Arch Med Search. 2002;33:330-42.
- Faria NR, Azevedo R do S da S, Kraemer MUG, Souza R, Cunha MS, Hill SC, et al. Zika virus in the Americas: Early epidemiological and genetic findings. Science [Internet]. 2016;5036(March):aaf5036. Available from:
- http://science.sciencemag.org/content/early/2016/03/23/science.aaf5036.abstract
- Staples JE, Breiman RF, Powers AM. Chikungunya Fever: An Epidemiological Review of a Re-Emerging Infectious Disease. Clin Infect Dis [Internet]. 2009;49(6):942–8. Available from: http://cid.oxfordjournals.org/lookup/doi/10.1086/605496
- 464 4. World Health Organization (WHO) Regional Office for South-East Asia. Dengue: guidelines for diagnosis, treatment, prevention, and control. Special Programme for Research and Training in Tropical Diseases. 2009.
- Gubler DJ. Dengue/dengue haemorrhagic fever: history and current status. Novartis Found Symp [Internet]. 2006;277:3-16-22, 71-3, 251-3. Available from: http://europepmc.org/abstract/MED/17319151
- 470 6. Brady OJ, Gething PW, Bhatt S, Messina JP, Brownstein JS, Hoen AG, et al. Refining the Global Spatial Limits of Dengue Virus Transmission by Evidence-Based Consensus. PLoS Negl Trop Dis. 2012;6(8).
- 7. Bhatt S, Gething PW, Brady OJ, Messina JP, Farlow AW, Moyes CL, et al. The global distribution and burden of dengue. Nature [Internet]. 2013;496(7446):504–7. Available from: http://dx.doi.org/10.1038/nature12060
- Khan K, Bogoch I, Brownstein JS, Miniota J, Nicolucci A, Hu W, et al. Assessing the origin of and potential for international spread of chikungunya virus from the Caribbean. PLoS Curr [Internet]. 2014;6:1–11. Available from:
- http://www.pubmedcentral.nih.gov/articlerender.fcgi?artid=4055609&tool=pmcentrez&rendertype=abstract
- Perkins TA, Metcalf CJE, Grenfell BT, Tatem AJ. Estimating drivers of autochthonous transmission of Chikungunya virus in its invasion of the Americas. PLoS Curr.
 2015;7(OUTBREAKS):1–26.
- Nsoesie EO, Kraemer MUG, Golding N, Pigott DM, Brady OJ, Moyes CL, et al. Global distribution and environmental suitability for chikungunya virus, 1952 to 2015. Eurosurveillance. 2016;21(20).
- 487 11. PAHO. Regional Zika Epidemiological Update (Americas) August 25, 2017 [Internet]. Pan
 488 American Health Organization. 2017 [cited 2017 Dec 4]. Available from:
 489 http://www.paho.org/hq/index.php?option=com_content&view=article&id=11599:regional490 zika-epidemiological-update-americas&Itemid=41691&lang=en
- 491 12. Bjornstad ON, Finkenstadt BF, Grenfell BT. Dynamics of measles epidemics: Estimating scaling of transmission rates using a Time series SIR model. Ecol Monogr. 2002;72(2):169–84.
- 494 13. Coburn BJ, Wagner BG, Blower S. Modeling influenza epidemics and pandemics: insights into the future of swine flu (H1N1). BMC Med [Internet]. 2009;7(1):30. Available from: http://bmcmedicine.biomedcentral.com/articles/10.1186/1741-7015-7-30
- 497 14. Kucharski AJ, Funk S, Eggo RM, Mallet H, Edmunds WJ, Nilles EJ. Transmission dynamics of Zika virus in island populations: a modelling analysis of the 2013 14 French Polynesia outbreak. bioRxiv. 2016;1–15.
- The state of the s
- 504 16. Eisen L, Monaghan AJ, Lozano-Fuentes S, Steinhoff DF, Hayden MH, Bieringer PE. The impact of temperature on the bionomics of Aedes (Stegomyia) aegypti, with special reference to the cool geographic range margins. J Med Entomol [Internet]. 2014;51(3):496–516. Available

- from: http://www.ncbi.nlm.nih.gov/pubmed/24897844
- 508 17. Rueda LM, Patel KJ, Axtell RC, Stinner RE. Temperature-Dependent Development and Survival
 509 Rates of Culex quinquefasciatus and Aedes aegypti (Diptera: Culicidae). J Med Entomol
 510 [Internet]. 1990;27(5):892–8. Available from: https://academic.oup.com/jme/article511 lookup/doi/10.1093/jmedent/27.5.892
- 512 18. Tun-Lin W, Burkot TR, Kay BH. Effects of temperature and larval diet on development rates and survival of the dengue vector Aedes aegypti in north Queensland, Australia. Med Vet Entomol. 2000;14(1):31–7.
- 515 19. Kakimura K, Matsuse IT, Takahashi H, Fukuda T, Suzuki K, Aratani M, et al. Effect of temperature on the development of Aedes aegypti and Aedes albopictus. Med Entomol Zool. 2002;53(1):53–8.
- 518 20. Beserra EB, Fernandes CRM, Silva SA de O, Silva L a. Da, Santos JW Dos. Efeitos da
 519 temperatura no ciclo de vida, exigências térmicas e estimativas do número de gerações anuais
 520 de Aedes aegypti (Diptera, Culicidae). Iheringia Série Zool [Internet]. 2009;99(2):142-8.
 521 Available from: http://www.scielo.br/scielo.php?script=sci_arttext&pid=S0073522 47212009000200004&lng=pt&nrm=iso&tlng=pt
- 523 21. Couret J, Dotson E, Benedict MQ. Temperature, larval diet, and density effects on development rate and survival of Aedes aegypti (Diptera: Culicidae). PLoS One. 2014;9(2).
- Watts DM, Burke DS, Harrison BA, Whitmire RE, Nisalak A. Effect of temperature on the vector efficiency of Aedes aegypti for dengue 2 virus. Am J Trop Med Hyg. 1987;36(1):143–527
- 528 23. McLean DM, Clarke AM, Coleman JC, Montalbetti CA, Skidmore AG, Walters TE, et al. Vector capability of *Aedes aegypti* mosquitoes for California encephalitis and dengue viruses at various temperatures. Can J Microbiol [Internet]. 1974;20(2):255–62. Available from: http://www.nrcresearchpress.com/doi/abs/10.1139/m74-040
- Altizer S, Dobson A, Hosseini P, Hudson P, Pascual M, Rohani P. Seasonality and the dynamics of infectious diseases: Seasonality and infectious diseases. Ecol Lett. 2006 Mar;9(4):467–84.
- 534 25. Mordecai EA, Cohen JM, Evans M V., Gudapati P, Johnson LR, Lippi CA, et al. Detecting the impact of temperature on transmission of Zika, dengue, and chikungunya using mechanistic models. PLoS Negl Trop Dis. 2017;11(4).
- Yang HM, Macoris MLG, Galvani KC, Andrighetti MTM, Wanderley DM V. Assessing the effects of temperature on dengue transmission. Epidemiol Infect. 2009;137(8):1179–87.
- Yang HM, Boldrini JL, Fassoni AC, Freitas LFS, Gomez MC, Lima KKB de, et al. Fitting the
 Incidence Data from the City of Campinas, Brazil, Based on Dengue Transmission Modellings
 Considering Time-Dependent Entomological Parameters. PLoS One [Internet].
 2016;11(3):e0152186. Available from: http://dx.plos.org/10.1371/journal.pone.0152186
- 543 28. Heffernan JM, Smith RJ, Wahl LM. Perspectives on the basic reproductive ratio. J R Soc Interface. 2005;2(4):281–93.
- 545 29. Mordecai E, Cohen J, Evans M V, Gudapati P, Johnson LR, Miazgowicz K, et al. Temperature determines Zika, dengue and chikungunya transmission potential in the Americas. 2016 Jul. Report No.: biorxiv;063735v1.
- 548 30. Duong V, Lambrechts L, Paul RE, Ly S, Lay RS, Long KC, et al. Asymptomatic humans transmit dengue virus to mosquitoes. Proc Natl Acad Sci [Internet]. 2015;112(47):14688–93. Available from: http://www.pnas.org/lookup/doi/10.1073/pnas.1508114112
- 551 31. Appassakij H, Khuntikij P, Kemapunmanus M, Wutthanarungsan R, Silpapojakul K. Viremic profiles in asymptomatic and symptomatic chikungunya fever: A blood transfusion threat? Transfusion. 2013;53(10 PART 2):2567–74.
- Murphy BR, Whitehead SS. Immune Response to Dengue Virus and Prospects for a Vaccine.
 Annu Rev Immunol [Internet]. 2011;29(1):587–619. Available from:
 http://www.annualreviews.org/doi/10.1146/annurev-immunol-031210-101315
- Weaver SC, Osorio JE, Livengood JA, Chen R, Stinchcomb DT. Chikungunya virus and prospects for a vaccine. Expert Rev Vaccines [Internet]. 2012;11(9):1087–101. Available from: http://www.tandfonline.com/doi/full/10.1586/erv.12.84
- Kucharski AJ, Funk S, Eggo RM, Mallet H-P, Edmunds WJ, Nilles EJ. Transmission Dynamics of
 Zika Virus in Island Populations: A Modelling Analysis of the 2013–14 French Polynesia

562 Outbreak. Barker CM, editor. PLoS Negl Trop Dis. 2016 May;10(5):e0004726.

Le Menach A, McKenzie FE, Flahault A, Smith DL. The unexpected importance of mosquito oviposition behaviour for malaria: non-productive larval habitats can be sources for malaria transmission. Malar J [Internet]. 2005;4:23. Available from: http://www.pubmedcentral.nih.gov/articlerender.fcgi?artid=1164431&tool=pmcentrez&ren

- dertype=abstract
 36. Palamara GM, Childs DZ, Clements CF, Petchey OL, Plebani M, Smith MJ. Inferring the temperature dependence of population parameters: The effects of experimental design and inference algorithm. Ecol Evol. 2014;4(24):4736–50.
- Ferkins TA. Retracing Zika's footsteps across the Americas with computational modeling.
 Proc Natl Acad Sci [Internet]. 2017;114(22):5558-60. Available from:
 http://www.pnas.org/lookup/doi/10.1073/pnas.1705969114

- Wesolowski A, Qureshi T, Boni MF, Sundsøy PR, Johansson MA, Rasheed SB, et al. Impact of human mobility on the emergence of dengue epidemics in Pakistan. Proc Natl Acad Sci [Internet]. 2015;112(38):11887–92. Available from: http://www.pnas.org/lookup/doi/10.1073/pnas.1504964112
- Zhang Q, Sun K, Chinazzi M, Pastore y Piontti A, Dean NE, Rojas DP, et al. Spread of Zika virus in the Americas. Proc Natl Acad Sci [Internet]. 2017;114(22):E4334-43. Available from: http://www.pnas.org/lookup/doi/10.1073/pnas.1620161114
 - 40. R Development Core Team. R: A Language and Environment for Statistical Computing [Internet]. Vienna, Austria: R Foundation for Statistical Computing; 2014. Available: http://www.R-project.org

APPENDIX

587

588

589

590

591

592

593

594

595

596

597

598

599

600

601

602

603

604

605

606

607

608

609

Starting Conditions

The model requires estimates of the mosquito-to-human ratio and the number of initially infectious humans and vectors to initiate each simulation. For these initial conditions, we used measures provided in previous models. In a model of the ZIKV outbreak in French Polynesia from 2013-2014, Kucharski et al. provided marginal posterior estimates for the proportion of initially infectious mosquitoes and the number of initially infectious humans on each island (34). We digitized the data for Tahiti and calculated the weighted average to arrive at estimates of 0.015 for the proportion of initially infectious vectors. Kucharski et al. estimated the mean number of initially infectious humans to be 450 (34). Assuming the 2012 population size of 183,645 for Tahiti, we arrived at an estimate of 0.0025 for the proportion of initially infectious humans. The literature on the ratio of mosquitoes to humans is limited. One model (35) that measured mosquito oviposition behavior adopted a patch modeling framework in which the overall ratio of mosquitoes to humans was equal to two, which we adopted here. With estimates for the mosquito-to-human ratio and the number of initially infectious individuals and vectors, we were able to calibrate our model. The total human population size, N_H , was set to a constant 10,000. Based on the proportion derived from (34), 25 individuals were initially infectious and the remaining population (9,975 individuals) was completely susceptible. E_H and R_H were initially set to zero.

611

612

613

614

615

616

617

618

619

620

621

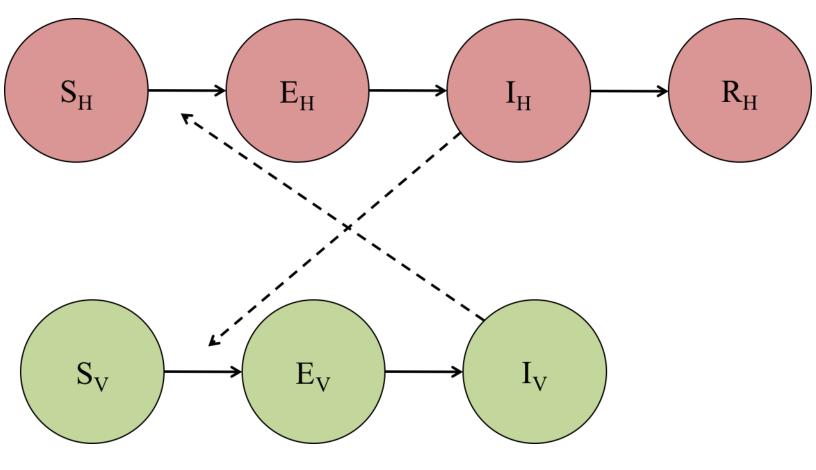
622

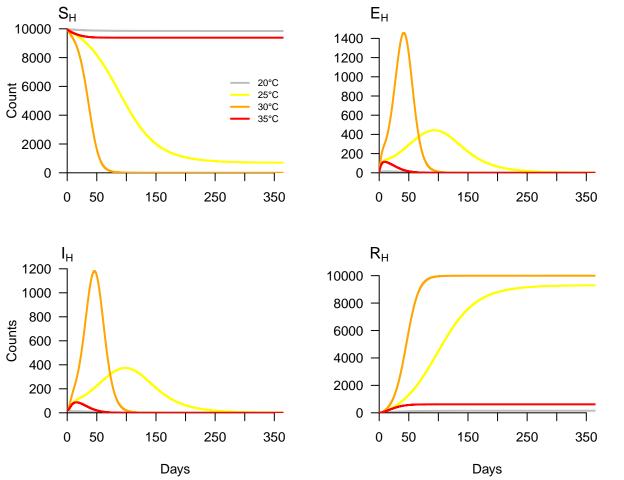
623

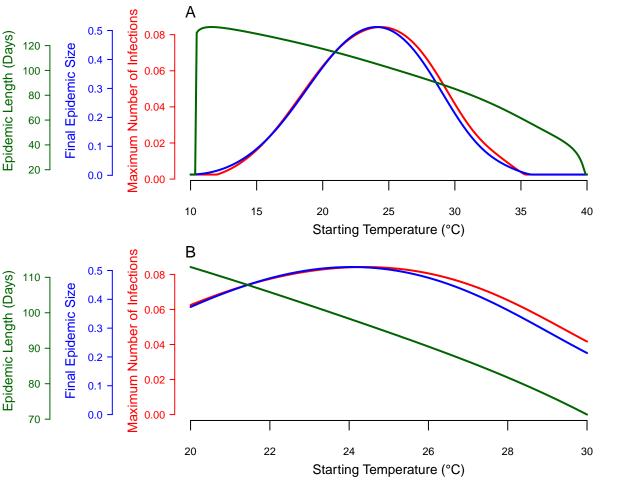
624

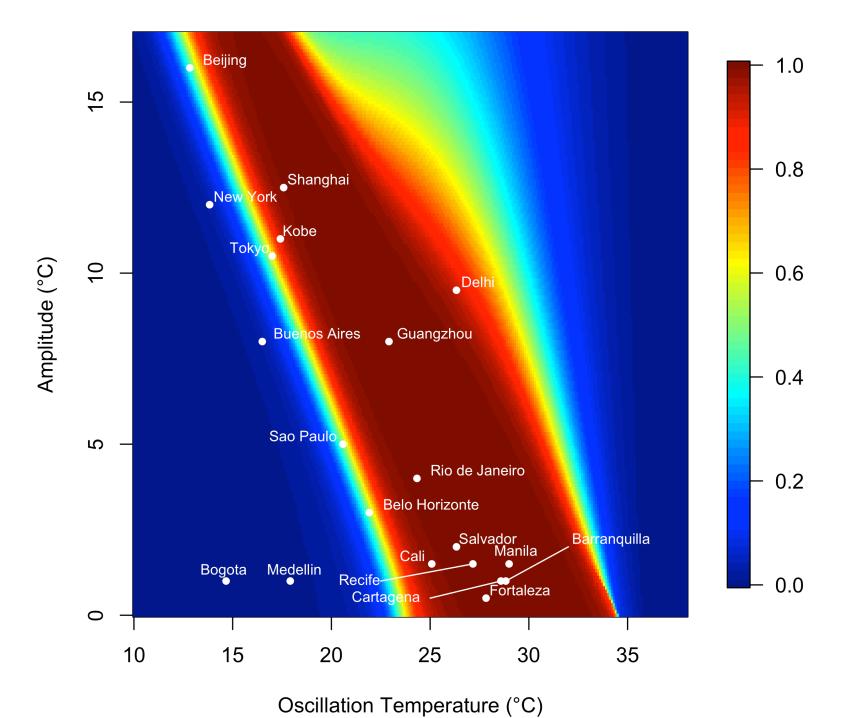
Since the carrying capacity and adult mosquito mortality rate were both dependent on temperature, the mosquito population size was subject to temperature effects. We assumed that the carrying capacity was greatest at 29°C (based on studies by Mordecai et al., 2016 and Le Menach et al., 2005) and totaled 20,000. To equilibrate the model, we set the initial mosquito population size (M_0) to the carrying capacity calculated from eq. 8 at the starting temperature. The quantity of initially infectious mosquitoes was calculated as 1.5% of the starting population size (34). The remaining mosquitoes (98.5%) were susceptible. The initial conditions were thus: $(S_V, E_V, I_V, S_H, E_H, I_H, R_H)_0 = (0.985M_0, 0, 0.015M_0, 9975, 0, 25, 0)$ Simulations Simulations were performed using a temperature-sensitive mechanistic modeling framework developed in C++. Code and supporting documentation for this model can be accessed at https://github.com/jhuber3/temperature-sensitive-sir.

Simulation outputs were processed in the R Programming Language 4.3.1 (40).









Temperature (°C)